Synthesis and Physicochemical Characterization of Protonated and Deprotonated Forms in Heteroleptic Lanthanide(III) Porphyrinate Double-Deckers. X-ray Structure of $Gd^{III}H(oep)(tpp)$ at 298 and 21 K

Georgios A. Spyroulias,[†] Catherine P. Raptopoulou,[‡] Dominique de Montauzon,[§] Alain Mari,[§] René Poilblanc,[§] Aris Terzis,[‡] and Athanassios G. Coutsolelos*,[†]

Laboratory of Bioinorganic Coordination Chemistry, Department of Chemistry, School of Science, University of Crete, P.O. Box 1470, 714 09 Heraklion, Crete, Greece, Institute of Materials Science, NCSR "Demokritos", 153 10 Aghia Paraskevi, Athens, Greece, and Laboratoire de Chimie de Coordination, CNRS, UPR 8241 liée par convention à l'Université Paul Sabatier et à l'Institut Polytechnique de Toulouse, 205 Route de Narbonne, 31077 Toulouse Cedex, France

Received July 18, 1997

The synthesis, spectroscopic characterization, and electrochemical study of eleven heteroleptic and their corresponding homoleptic lanthanide sandwiches are reported. Studies in solution have been carried out in solvents of different basicity, in order to elucidate the equilibrium between the protonated and deprotonated form of these complexes. The investigated compounds are represented by the formulas $Ln^{III}H(oep)(tpp)$ and $[Ln^{III}(oep)(tpp)]^-$ corresponding to the protonated and deprotonated forms, respectively (in the case of heteroleptic), and the formulas $Ln^{III}H(tpp)_2$ and $[Ln^{III}(tpp)_2]^-$ (in the case of the homoleptic porphyrin double-deckers), where Ln Nd, ..., Lu (except Pm), oep = 2,3,7,8,12,13,17,18-octaethylporphyrinate, and tpp = 5,10,15,20-tetraphenylporphyrinate). Various spectroscopic methods are used for the physicochemical characterization of the title complexes. The electronic spectra of the complexes above present different features in CH_2Cl_2 and in DMF. In the latter solvent they reveal features similar to those of the analogous actinide(IV) porphyrin double-decker. The electrochemical studies carried out in CH_2Cl_2 and THF demonstrate clearly that the redox behavior of the double-deckers, heteroleptic or homoleptic, is strongly dependent on the proton on the porphyrinic core. In CH_2Cl_2, four reversible oxidation processes and two quasi-reversible waves are observed for the protonated species in both homo- and heteroleptic double-deckers. In contrast, two oxidations and two reductions are observed in THF for the homoleptic derivatives, while the corresponding heteroleptic ones undergo three oxidations and one reduction process. The structure of the new heteroleptic double-decker $Gd^{III}H(oep)(tpp)$ was determined by X-ray diffraction at 298 and 21 K. Both structures are compared with the first analogous structure of $Sm^{III}H(oep)(tpp)$. According to the spectroscopic and structural data reported for the heteroleptic protonated derivatives, the oep macrocycle is the favored binding site of the proton in solutions as well as in the solid state.

Introduction

Since the elucidation of the reaction center of *Rhodopseudomonas viridis*,[1] by X-ray diffraction analysis, research into the synthesis and physicochemical characterization of lanthanide(III),[2−33] actinide(IV),[9,18,34,35] Zr(IV),[12,36,37] and Hf(IV),[12,37] porphyrin double-deckers has displayed remarkable growth. The extensive structural and electronic similarities between the bacterial

* Author to whom correspondence should be addressed. Tel.: +30 81 393636. Fax: +30 81 210951 (+30 81 393804 on PC modem). E-mail: coutsole@ikaros.edu.uch.gr.

[†] University of Crete.

[‡] Institute of Materials Science.

[§] CNRS and Université Paul Sabatier.

(1) (a) Deisenhofer, J.; Epp, O.; Miki, K.; Huber, R. Michel, H. *Nature (London)* **1985**, *318*, 618−624. (b) Deisenhofer, J.; Epp, O.; Miki, K.; Huber, R.; Michel, H. *J. Mol. Biol.* **1984**, *180*, 385−398.

(2) Buchler, J. W.; Kapellmann, H. G.; Knoff, M.; Lay, K-L.; Pfeifer, S. *Z. Naturforsch.* **1983**, *38B*, 1339.

(3) Buchler, J. W.; De Cian, A.; Fischer, J.; Kihn-Botulinski, M.; Paulus, H.; Weiss, R. *J. Am. Chem. Soc.* **1986**, *108*, 3652−3659.

(4) Buchler, J. W.; Scharbert, B. *J. Am. Chem. Soc.* **1988**, *110*, 4272−4276.

(5) Buchler, J. W.; De Cian, A.; Fischer, J.; Kihn-Botulinski, M.; Weiss, R. *Inorg. Chem.* **1988**, *27*, 339−345.

(6) Buchler, J. W.; Elsässer, K.; Kihn-Botulinski, M.; Scharbert, B. *Angew. Chem., Int. Ed. Engl.* **1986**, *25*, 286−287.

(7) Duchowski, J. K.; Bocian, D. F. *J. Am. Chem. Soc.* **1990**, *112*, 3312−3318.

(8) Yau, X.; Holten, D. *J. Phys. Chem.* **1988**, *92*, 409−414.

(9) Bisel, O.; Rodriguez, J.; Holten, D.; Girolami, G. S.; Milam, S. N.; Suslick, K. S. *J. Am. Chem. Soc.* **1990**, *112*, 4075−4077.

(10) Girolami, G. S.; Milam, S. N.; Suslick, K. S. *Inorg. Chem.* **1987**, *26*, 343−344.

(11) Buchler, J. W.; Hammerschmitt, P.; Kaufeld, I.; Löffler, J. *Chem. Ber*. **1991**, *124*, 2151−2159.

(12) Buchler, J. W.; De Cian, A.; Fischer, J.; Hammerschmitt, P.; Weiss, R. *Chem. Ber.* **1991**, *124*, 1051−1058.

(13) Buchler, J. W.; Hüttermann, J.; Löffler, J. *Bull. Chem. Soc. Jpn.* **1988**, *61*, 71−77.

(14) Buchler, J. W.; Kihn-Botulinski, M.; Scharbert, B. *Z. Naturforsch.* **1988**, *43B*, 1371−1380.

(15) Buchler, J. W.; Löffler, J. *Z. Naturforsch*. **1990**, *45B*, 531−542.

(16) Donohoe, R. J.; Duchowski, J. K.; Bocian, D. F. *J. Am. Chem. Soc.* **1988**, *110*, 6119−6124.

(17) Perng, J.-H.; Duchowski, J. K.; Bocian, D. F. *J. Phys. Chem.* **1990**, *94*, 6684−6691.

(18) Girolami, G. S.; Milam, S. N.; Suslick, K. S. *J. Am. Chem. Soc.* **1988**, *110*, 2011−2012.

(19) Bilsel, O.; Rodriguez, J.; Holten, D. *J. Phys. Chem.* **1990**, *94*, 3508−3512.

(20) Buchler, J. W.; De Cian, A.; Fischer, J.; Hammerschmitt, P.; Löffler, J.; Scharbert, B.; Weiss, R. *Chem. Ber*. **1989**, *122*, 2219−2228.

(21) Duchowski, J. K.; Bocian, D. F. *Inorg. Chem.* **1990**, *29*, 4158−4160.

10.1021/ic970879s CCC: $18.00
Published on Web 04/02/1999

photosynthetic reaction center and the porphyrin sandwich-like complexes gave rise to the synthesis of new double-deckers.[19−22,28−34,37] The importance of the above complexes stems from the existence of strong $\pi-\pi$ interactions between the two macrocycles. The vast majority of the lanthanide porphyrin double-decker complexes reported thus far are homoleptic, with only sporadic reports of the synthesis of some heteroleptic porphyrin sandwich-like complexes with Ce(IV),[19−21] La(III),[23] and Eu(III)[14] ions by Buchler and co-workers. Moreover, the complex of Ce(IV)[20] has been thoroughly investigated, including an X-ray structure determination. Unfortunately, the reported synthetic route and the employed isolation procedure for heavier lanthanide ions led to a mixture of products.[14] Recently, our group has presented the synthesis, spectroscopic characterization, and the first structure of a trivalent lanthanide porphyrin double-decker, $Sm^{III}H(oep)(tpp)$.[31] In the present study, the synthetic and purification/isolation route previously reported by Buchler et al.[20] has been modified to yield analytically pure double-deckers $Ln^{III}(oep)_2$, $Ln^{III}H(oep)(tpp)$, and $Ln^{III}H(tpp)_2$ (where Ln = Nd, ..., Lu, except Pm) and in some cases the triple-decker $Ln^{III}_2(oep)_3$ (where Ln = Nd, ..., Tb). The presence of protonated forms for the homoleptic or heteroleptic double-deckers has been mentioned before but never directly proved by any spectroscopic method and/or compared along the series (homo- versus heteroleptics). The goal of the present work is the facile synthesis, isolation, and full characterization of analytically pure, heteroleptic complexes, free from partially oxidized protonated/deprotonated complexes. A thorough investigation of eleven protonated and deprotonated heteroleptic double-deckers provides direct and unambiguous evidence of the presence of the proton and its relative affinity to the macrocycles used.

Results

In solution, the equilibrium between the protonated and deprotonated form of the title complexes is solvent-dependent. Equilibrium 1 has been postulated for all the porphyrin double-decker complexes investigated by UV−visible, ^{1}H-NMR, and electrochemical studies. It has been previously suggested in the UV−visible spectroscopic study of the Sm(III) complex.[31]

$$\underset{\mathbf{A}}{Ln^{III}H(porph)(porph')} \underset{}{\overset{\text{basic solvent, } -H^+}{\rightleftharpoons}} \underset{\mathbf{B}}{[Ln^{III}(porph)(porph')]^-} \quad \text{where porph} = \text{or} \neq \text{porph}' \tag{1}$$

In electrochemistry, two solvents were chosen: CH_2Cl_2, in which the protonated form **A** is dominant, and THF, in which equilibrium 1 favors the deprotonated form **B**. A comparison of the redox potentials between the heteroleptic and homoleptic complexes provides information about the nature of the electron transfer and the nature of the species generated during the electrochemical process. Selected monoporphyrinates with the molecular formula $Ln^{III}(tpp)acac$ (Ln = Sm, Eu, Gd) were also studied in order to understand differences in the redox properties arising $\pi-\pi$ interactions in the corresponding bis-porphyrinates (homo- and heteroleptic). With the exception of the Lu(III) complexes,[32] all others display a paramagnetic behavior due to the unpaired electrons of the rare-earth elements. An EPR hyperfine structure was observed in all cases (except gadolinium and europium) with two observable groups of eight nonsymmetrical peaks. In the case of gadolinium, the EPR spectra exhibit characteristic features of an S state ion (Gd ground state: $^7S_{8/2}$). Finally, the Gd(III) heteroleptic representative, $Gd^{III}H(oep)(tpp)$, was studied by X-ray diffraction both at 298 and at 21 K in an attempt to locate the proton in question.

Experimental Section

General Information. Dichloromethane (CH_2Cl_2) and 1,2,4-trichlorobenzene (1,2,4-tcb) were purchased from Riedel-de Häen and Aldrich, respectively, and used as received. Tetrahydrofuran (THF) was purchased from Merck and distilled under an argon atmosphere over a mixture of sodium/benzophenone. Tetra-*n*-butylammonium perchlorate (TBAP) was purchased from Fluka (electrochemical grade). All syntheses were performed under an argon stream atmosphere using Schlenk-tube techniques. Pentanedione [acac(H)] and all lanthanide salts in the form of chlorides or nitrates were purchased from Aldrich and used as received. The $(tpp)H_2$ free base was synthesized according to a reported method,[38] $(oep)H_2$ by a modified process,[39] and the metalation reactions were performed by the acetylacetonate method.[40]

Instrumentation. Absorption spectra were collected on a Perkin-Elmer Lambda 6 (or a Perkin-Elmer 330 for NIR) grating spectrophotometer. Spectra for ϵ measurements were recorded in CH_2Cl_2 (solutions of 0.05×10^{-3} M). IR spectra were recorded on a Perkin-Elmer FT series 1760 spectrophotometer in CsI pellets. EPR spectra were recorded at X-band frequency with a Bruker spectrometer ER 200D-SRC at 298 or 77 K, as pure solid, and in CH_2Cl_2 or DMF solutions. Signal intensities and g values were calibrated with a standard diphenylpicrylhydrazyl (dpph) sample ($g = 2.0036$). Magnetic susceptibility measurements on pure solids were recorded on a Quantum Design MPMS-5, SQUID magnetometer. Electrochemical measurements were carried out with a home-made potentiostat interfaced with a microcomputer. Positive feedback or the interrupt method was used to compensate for IR drop. Electrochemical experiments were performed in an airtight three-electrode cell connected to a vacuum/argon line. The cell was degassed and filled according to standard vacuum techniques. The reference electrode consisted of a SCE separated from the solution by a bridge compartment filled with the same solvent and supporting electrolyte solution as used in the cell. The counter electrode was a spiral one of ca. 1 cm^2 apparent surface area, made from ca. 8

(22) Chabach, D.; Tahiri, M.; De Cian, A.; Fischer, J.; Weiss, R.; El Maloul Bibout, M. *J. Am. Chem. Soc.* **1995**, *117*, 8548−8556.
(23) Buchler, J. W.; Kihn-Botulinski, M.; Scharbert, B.; Löffler, J. *New J. Chem.* **1992**, *16*, 545−553.
(24) Buchler, J. W.; Löffler, J.; Wicholas, M. *Inorg. Chem.* **1992**, *31*, 524−526.
(25) Buchler, J. W.; Kihn-Botulinski, M.; Löffler, J.; Wicholas, M. *Inorg. Chem.* **1989**, *28*, 3770−3772.
(26) Duchowski, J. K.; Bocian, D. F. *J. Am. Chem. Soc.* **1990**, *112*, 8807−8811.
(27) Davoras, E.; Spyroulias, G. A.; Mikros, E.; Coutsolelos, A. G. *Inorg. Chem.* **1994**, *33*, 3430−3434.
(28) Lachkar, M.; De Cian, A.; Fischer, J.; Weiss, R. *New J. Chem.* **1988**, *12*, 729−731.
(29) Chabach, D.; Lachkar, M.; De Cian, A.; Fischer, J.; Weiss, R. *New J. Chem.* **1992**, *16*, 431−433.
(30) Moussavi, M.; De Cian, A.; Fischer, J.; Weiss, R. *Inorg. Chem.* **1986**, *25*, 2107−2108.
(31) Spyroulias, G. A.; Coutsolelos, A. G.; Raptopoulou, C.; Terzis, A. *Inorg. Chem.* **1995**, *34*, 2476−2479.
(32) Spyroulias, G. A.; Coutsolelos, A. G. *Inorg. Chem.* **1996**, *35*, 1382−1385.
(33) Spyroulias, G. A.; Coutsolelos, A. G.; de Montauzon, D.; Poilblanc, R. *J. Coord. Chem.* **1996**, *39*, 89−96.
(34) Kadish, K. M.; Moninot, G.; Hu, Y.; Dubois, D.; Ibnlfassi, A.; Barbe, J.-M.; Guilard, R. *J. Am. Chem. Soc.* **1993**, *115*, 8153−8166.
(35) Bilsel, O.; Rodriguez, J.; Milam, S. N.; Gorlin, P. A.; Girolami, G. S.; Suslick, K. S.; Holten, D. *J. Am. Chem. Soc.* **1992**, *114*, 6528−6538.
(36) Kim, K.; Lee, W. S.; Kim, H. J.; Cho, S. H.; Girolami, G. S.; Gorlin, P. A.; Suslick, K. S. *Inorg. Chem.* **1991**, *30*, 2652−2656.
(37) Guilard, R.; Barbe, J.-M.; Ibnlfassi, A.; Zrineh, A.; Adamian, V. A.; Kadish, K. *Inorg. Chem.* **1995**, *34*, 1472−1481.
(38) Adler, A. D.; Longo, F. R.; Kampus, F.; Kim, J. *J. Inorg. Nucl. Chem.* **1967**, *32*, 476.
(39) Whittlock, H. W.; Hanauer, R. *J. Org. Chem.* **1968**, *33*, 2169−2175.
(40) Wong, C. P.; Veinteicher, R. F.; Hoorocks, W.; Dew, Jr. *J. Am. Chem. Soc.* **1974**, *96*, 4149−4151.

cm of a 0.5 mm diameter platinum wire. The working electrode was a 1 mm diameter Pt disk and the RDE (rotating disk electrode) was a 2 mm diameter Pt disk (Tacussel EDI). With the above reference and bridge system $E° = 0.54$ V was obtained for 2 mM ferrocene solutions in 0.1 M CH_2Cl_2/$n$$Bu_4NBF_4$.

Synthesis of Neutral Complexes [Ln^{III}H(oep)(tpp) and Ln^{III}H(tpp)$_2$]. Lanthanide(III) monoporphyrinates, Ln^{III}(tpp)acac, with Ln = Nd, ..., Lu were prepared according to well established experimental procedures.[40] The synthesis of the corresponding homo- and heteroleptic double-deckers Ln^{III}H(tpp)$_2$ and Ln^{III}H(oep)(tpp) was carried out as follows: The freshly prepared Ln^{III}(tpp)acac (0.500 g, 0.570 mmol) was refluxed in 1,2,4-trichlorobenzene for 3−5 h with 0.350 g (0.654 mmol) of Li_2(oep), prepared in situ according to the method published for the Sm^{III}H(oep)(tpp).[31] The reaction mixture was then allowed to cool to room temperature. The isolation of all the complexes was achieved in four column chromatography steps as follows.

First Chromatography Column. The reaction mixture was passed through a Al_2O_3 column (5 × 12 cm, type Basic I, activated at 150 °C overnight) using toluene as the eluant. Five fractions were collected. The first fraction [F1] contains the major quantity of Ln^{III}(oep)$_2$ contaminated by the free base (tpp)H_2 [probably generated by partial demetalation of the starting material Ln^{III}(tpp)acac], while the second fraction [F2] contains mainly (tpp)H_2 with traces of Ln^{III}(oep)$_2$ and Ln$^{III}_2$(oep)$_3$ (only where Ln = Nd, ..., Tb). The third fraction [F3] contains the major quantity of Ln$^{III}_2$(oep)$_3$ and traces of Ln^{III}(oep)$_2$, (tpp)H_2, and Ln^{III}H(oep)(tpp). The heteroleptic porphyrin double-decker was eluted in the fourth fraction [F4], although contaminated by traces of (tpp)H_2, Ln^{III}(oep)$_2$, and Ln$^{III}_2$(oep)$_3$. Finally, the homoleptic double-decker Ln^{III}H(tpp)$_2$ was eluted at the fifth fraction [F5] together with traces of the other two double-deckers Ln^{III}H(oep)(tpp) and Ln^{III}(oep)$_2$ and the unreacted free base (oep)H_2. At the end, the elution of Ln^{III}H(tpp)$_2$ was accelerated by using only CH_2Cl_2 as the eluant.

Second Chromatography Column. The [F1] fraction (essentially residual solution of 1,2,4-tcb, after evaporation of the toluene) was passed through a column of Al_2O_3 (5 × 12 cm, type Basic I, activated at 150 °C overnight) with a mixture of solvents, $PhCH_3$/hexane, 1:1 (v/v). The first fraction [F1.1] contains the free base (tpp)H_2 (at this stage 1,2,4-tcb is also eliminated), followed by a mixture of (tpp)H_2 and Ln^{III}(oep)$_2$ [F1.2]. Ln^{III}(oep)$_2$ was collected at the third fraction [F1.3] using $PhCH_3$ as the eluant. The procedure described was applied only to the complexes of Sm(III), Gd(III), and Dy(III), yielding analytically pure Ln^{III}(oep)$_2$ double-deckers.

Third Chromatography Column. In order to obtain pure Ln^{III}H(tpp)$_2$, which was eluted in the [F5] fraction, a new chromatographic separation employing by "dry" column of Al_2O_3 (type Basic I, 5 × 10 cm) was carried out with a mixture of solvents, petroleum ether/diethyl ether, 1:1 (v/v). The first fraction [F5.1] contains a mixture of (tpp)H_2, Ln^{III}(oep)$_2$, and Ln$^{III}_2$(oep)$_3$. The second fraction [F5.2] eluted with a mixture of solvents, diethyl ether/CH_2Cl_2, 100:1 (v/v), contains the heteroleptic complex Ln^{III}H(oep)(tpp), although contaminated with the above-mentioned [F5.1] traces. Pure Ln^{III}H(tpp)$_2$ was eluted with CH_2Cl_2. Recrystallization carried out by slow evaporation of saturated $PhCH_3$ solutions or using mixtures of solvents CH_2Cl_2/hexane 1:(5−10) (v/v) yielded a purple crystalline powder (the reaction yields for the series of complexes from Nd to Lu are between 4 and 28%.

Fourth Chromatography Column. The [F4] and [F5.1] fractions after concentration of the solution were again passed through a "dry" column of Al_2O_3 (type Basic I, 5 × 12 cm) and separation was effected by a mixture of four solvents, cyclohexane/petroleum ether/diethyl ether/acetone 9:9:1:1 (v/v), as first eluant. Ln^{III}(oep)$_2$, (tpp)H_2, Ln$^{III}_2$(oep)$_3$, and traces of the oxidized heteroleptic complex (formed under unknown conditions)[37] were eluted first, while the main quantity of the free base and the triple decker followed. Then, a mixture of solvents diethyl ether/CH_2Cl_2 with a ratio 100:1 (v/v) was used followed by the same mixture with the ratio of 100:10 (v/v). This process eliminates the remaining traces of the above compounds, especially the undesired oxidized heteroleptic double decker, while the Ln^{III}H(oep)(tpp) complex began to move from the top of the column. Finally, analytically pure Ln^{III}H(oep)(tpp) was obtained by using only CH_2Cl_2 (yield 5−35%). Recrystallization was carried out by slow evaporation of a saturated toluene solution or from mixtures of CH_2Cl_2/MeOH with a ratio of 1:(5−10) (v/v), yielding prismatic purple crystals.

Table 1. Summary of Crystal, Intensity Collection, and Refinement Data for LT and RT for Gd^{III}H(oep)(tpp)·CH_2Cl_2

empirical formula	$C_{81}H_{75}N_8Cl_2Gd$	$C_{81}H_{75}N_8Cl_2Gd$
formula weight	1388.64	1388.64
temperature, K	21	298
wavelength	Mo Kα 0.710 70	Mo Kα 0.710 70
space group	$P2_1/c$	$P2_1/c$
a (Å)	13.703(1)	13.780(1)
b (Å)	19.008(2)	19.410(1)
c (Å)	25.807(3)	26.183(2)
β, deg	101.734(3)	101.938(2)
V (Å^3)	6581.4(1)	6851.5(8)
Z	4	4
D_{calcd}/D_{measd} (Mg m^{-3})	1.401/1.39	1.346/1.32
abs. coeff (μ), mm^{-1}	1.100	1.057
max. abs. correction mode	1.63	1.24
no. of octants collected	$h, k, \pm l$	$\pm h, k, -l$
goodness-of-fit on F^2	1.162	1.133
R indices^a	R1 = 0.0733, wR2 = 0.1859^b	R1 = 0.0475, wR2 = 0.1152^b

^{a} $I > 2\sigma(I)$; 11 456 reflections; R1 based on F, wR2 based on F^2. ^{b} $R1 = \sum||F_o| - |F_c||/\sum|F_o|$; $wR2 = \{\sum[w(F_o^2 - F_c^2)^2]/\sum[wF_o^4]\}^{1/2}$.

Phenoxathiinylium Radical Cation. To a solution of 0.997 g (4.98 mmol) of phenoxathiin ($C_{12}H_8SO$) in 30 mL of CH_2Cl_2 under argon was added 0.65 mL (5.20 mmol) of $SbCl_5$. The solution was stirred for 15 min and filtrated, yielding 1.42 g (54%) violet powder of phenoxathiinylium hexachloroantimonate.

Oxidized Complexes. The chemically oxidized complexes were synthesized using phenoxathiinylium hexachloroantimonate in CH_2Cl_2 according to previously reported synthetic procedures.[41] A typical example is given below.

[Ln^{III}(oep)(tpp)]$^+$[SbCl$_6$]$^-$. A solution of 0.021 g (0.04 mmol) of phenoxathiinylium hexachloroantimonate in 10 mL of CH_2Cl_2 is added dropwise to a solution of 0.05 g (0.04 mmol) of Ln^{III}H(oep)(tpp). The solution is stirred for 30 min at room temperature and then concentrated. The crude solid residue was crystallized from $PhCH_3$/MeOH 1:5 (v/v). After filtration, 0.039 g (yield 62%) of cation radical species was collected [for the heteroleptic porphyrin complex with Gd(III)].

[Ln^{III}(tpp)$_2$]$^+$[SbCl$_6$]$^-$. The experimental procedure described above also is used for the corresponding homoleptic tpp complexes except that the crude solid was recrystallized from $PhCH_3$/hexane 1:5 (v/v), yielding 0.049 g (yield 65%) [for Gd(III)].

X-ray Structure Determination. Slow crystallization of Gd^{III}H(oep)(tpp) from a mixture of CH_2Cl_2/MeOH yielded purple prismatic crystals. A crystal with approximate dimensions 0.40 × 0.40 × 0.50 mm was mounted in the air and covered with epoxy glue. Diffraction measurements at room temperature (298 K) and at 21 K were taken on a Crystal Logic dual goniometer diffractometer using graphite-monochromated Mo radiation. Unit cell dimensions were determined and refined by using angular settings of 25 automatically centered reflections in the range $11° < 2\theta < 23°$ and are reported in Table 1. Intensity data were recorded using a $\theta-2\theta$ scan. Three standard reflections monitored every 97 reflections showed less than 3% variation and no decay. Lorentz, polarization, and ψ-scan absorption corrections were applied using Crystal Logic software. The structure was solved by direct methods using SHELXS-86[42] and refined full-matrix least-squares techniques on F^2 with SHELXL-93.[43] Important crystal data for both temperatures are given in Table 2; supplementary data are (i) for room temperature: $2\theta(\max) = 44°$, scan speed 4.5°/min, scan range 2.5 plus $\alpha_1\alpha_2$ separation; reflections collected/unique/used, 8638/8413 ($R_{int} = 0.0286$)/8379; parameters refined, 828; $F(000) = 2860$; $[\Delta/\sigma]_{max} = 0.023$; $[\Delta\rho]_{max}/[\Delta\rho]_{min}$, 1.084/−0.675 e Å^{-3}; R1/wR2/GOF (all data),

(41) Gans, P.; Marchon, J. C.; Reed, C. A.; Regnard, J. R. *New J. Chem.* **1981**, *5*, 203−206.
(42) Sheldrick, G. M. *SHELXS-86: Structure Solving Program*; University of Göttingen: Germany, 1986.
(43) Sheldrick, G. M. *SHELXS-93: Crystal Structure Refinement*; University of Göttingen: Germany, 1993.

Table 2. X-ray Data for $Gd^{III}H(oep)(tpp)$ at Room and Low Temperature; Data for the Corresponding Sm(III)[31] Complex Are Also Included

parameter	$Sm^{III}H(oep)(tpp)$	$Gd^{III}H(oep)(tpp)$ RT	$Gd^{III}H(oep)(tpp)$ LT
$N_1N_2N_3N_4$ (tpp)	1.470	1.450	1.430
Ln			
$N_5N_6N_7N_8$ (oep)	1.516	1.495	1.487
$4Np_{(oep)}-4Np_{(tpp)}$	2.986	2.945	2.917
distance$_{(oep)-(tpp)}$	3.535	3.501	3.454
N_1	2.489(4)	2.503(5)	2.485(5)
N_2	2.551(4)	2.540(5)	2.542(5)
N_3	2.603(5)	2.534(5)	2.537(5)
N_4	2.509(4)	2.520(5)	2.503(5)
Ln			
N_5	2.533(4)	2.479(5)	2.658(5)
N_6	2.555(4)	2.547(5)	2.531(6)
N_7	**2.619(5)**	**2.642(6)**	**2.461(6)**
N_8	2.553(4)	2.537(5)	2.539(5)
dihedral angle$_{(oep)-(tpp)}$	0.858	1.287	1.405

0.0685/0.1463/1.255; all H atoms were introduced at calculated positions as riding on carbon atoms and were refined isotropically; all non-H atoms were refined anisotropically (except for the solvent dichloromethane molecule, C_{66}, and C_{70} which were disordered and were treated isotropically). (ii) For low temperature: $2\theta(\max) = 55°$, scan speed 6.0°/min, scan range 2.9 plus $\alpha_1\alpha_2$ separation; reflections collected/unique/used, 15 736/15 128 ($R_{int} = 0.0364$)/15 120; parameters refined, 869; $F(000) = 2860$; $[\Delta/\sigma]_{max} = 0.208$; $[\Delta\rho]_{max}/[\Delta\rho]_{min}$, 3.148/−3.567 e Å^{-3}; R1/wR2/GOF (all data), 0.0987/0.2186/1.188; all H atoms were introduced at calculated positions as riding on carbon atoms and were refined isotropically; all non-H atoms were refined anisotropically. The solvent dichloromethane molecule was found disordered and was refined anisotropically at two different positions with occupancy fixed at 0.5.

Discussion

Synthesis. Two synthetic routes have been reported by Buchler and co-workers[14,20] describing the synthesis of lanthanide asymmetrical complexes. According to data reported, the $Eu^{III}H(oep)(tpp)$ complex[14] was isolated after seven steps of repeated chromatographic separations. The final product exhibits two major absorption maxima in the Soret band region. According to our findings, these UV−visible data signify the presence of a mixture of compounds, oxidized and neutral complexes. We herein present the UV−visible data for the protonated and deprotonated forms, **A** or **B**, in the above-mentioned equilibrium 1 (from Nd to Lu except Pm) which exhibit a single Soret band. The second band at 380 nm reported by Buchler[14] is probably due to the oxidized product $[Eu^{III}(oep)(tpp)]^{\bullet}$. This byproduct seems to appear under undefined conditions during the chromatographic procedures as that reported by Kadish et al.[37] To further confirm this, the chemically oxidized $[Eu^{III}(oep)(tpp)]^{\bullet}$ by an established procedure[41] and the product generated displays a singlet absorption band at 380 nm.

The direct reaction of the monoporphyrinates with the *in situ* prepared dilithium octaethylporphyrinate $[Li_2(oep)]$ occurs in boiling 1,2,4-trichlorobenzene and gives rise to a mixture of products including the homoleptic and heteroleptic double-decker derivatives (Figure 1). The presence of the tpp free base can be attributed to a side reaction of the lanthanide precursor, Ln^{III}(tpp)acac, which is likely demetalated under the employed experimental conditions. Traces of the oep triple-decker $Ln^{III}_2(oep)_3$ are also observed, probably formed by the so-called “raised by one-story reaction” of the homoleptic oep complex. In addition, a certain amount of Ln^{III}(oep)acac has been observed

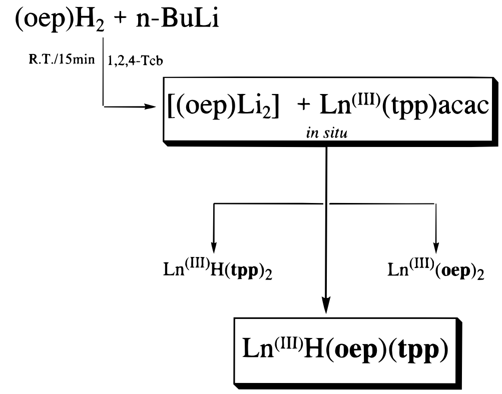

Figure 1. Reaction scheme for the synthesis of homoleptic and heteroleptic double-deckers.

which remained at the top of the column during the first chromatographic procedure, together with the tpp monoporphyrinate.

The Nature of the Complexes. a. Protonated Form or Not? There is a long debate about the nature of the lanthanide(III)-bis(porphyrinates) concerning the presence of a proton on the pyrrolic nitrogens and how their physicochemical properties could be affected from this fact.[2−6,11−15,23,31−33] Although there is no doubt about its presence, as different spectroscopical features have been detected after abstraction of this proton under a variety of conditions in solution (basic solvents, reagents such as $[NBu_4]^-$, electrooxidation, and/or chemical oxidation, etc.) only recently has our group presented its direct evidence through ^{1}H-NMR spectroscopy.[32] Also, according to our experimental data, the synthetic and purification/isolation procedure plays a crucial role on the nature of the isolated complexes in order to be free from any oxidized species.

Concerning the symmetrical Ln(III) bis(porphyrinates), each group of the four pyrrolic nitrogens is equally susceptible to retain the proton. This is not the case for the asymmetrical Ln^{III}-bis(porphyrinates) as presented below. For this reason, the challenging aspect to locate the proton in question becomes a necessity in the effort of understanding the structure−property relationship of those complexes. The equilibrium based on UV−visible data already postulated in earlier work[31] has been extended to the whole series by the complete study of their UV−visible and electrochemistry data in various solvents. This equilibrium is solvent-dependent and in solutions of CH_2Cl_2, $CHCl_3$, and $PhCH_3$, the protonated form is present, while in basic solvents such as DMF and pyridine, the deprotonated form dominates. High-resolution ^{1}H-NMR studies for the Lu(III) complexes,[32] the diamagnetic member of the families of $Ln^{III}H(tpp)_2$ and $Ln^{III}H(oep)(tpp)$, suggests that in $CDCl_3$ solutions the complexes (homo- and heteroleptics) are protonated. In contrast, for the same derivatives their spectra in DMF-d_7 clearly demonstrates the complete disappearance of the N−H signal for both kinds of complexes; hence, the complexes are deprotonated (see Supporting Information). Moreover, in the case of the heteroleptic $Ln^{III}H(oep)(tpp)$, two N−H signals have been detected; one attributed to the proton attached on the tpp porphyrin ring and the other to the oep ring. Based on the integration of the signals’ intensities (the sum of the two peaks corresponds to one proton), a ratio of $N-H_{tpp}/N-H_{oep}$ equal to 1:4.3 was deduced.[32]

b. Cation Radicals or Not? Another interesting observation that arose from our systematic studies on both the families of eleven homoleptic Ln^{III}bis(tetraphenylporphyrinato) and their heteroleptic bis(octaethyltetraphenylporphyrinates) is the oxidation of the complexes during the preparation of the complexes, which has also been reported in the literature.[37] The reagents used and the methods adopted and described above avoid any undesired oxidized product. Magnetic susceptibility measurements yielded values of magnetic moments typical for the +3 oxidation state. The nature of the complexes has been investigated and the absence of π-cation radicals has been verified through ESR spectroscopy in solutions and pure solids. All title compounds were studied in the solid state as well as in toluene or CH_2Cl_2 solution both at 298 and 98 K. For all complexes, except for the case of Gd(III) and Eu(III), the observed signal is due to the presence of electron spin density on the porphyrin ring. It exhibits a hyperfine structure with two groups of eight nonsymmetrical peaks with a peak to peak separation Δpp = 16.9−17.4 G, as has already been reported for Sm^{III}H(oep)(tpp).[31] The europium homo- and heteroleptic complexes exhibit a broad structureless signal at $g = 1.958$ and 2.138, respectively (see Supporting Information). The absence of the hyperfine structure has also been reported in the case of the homoleptic Eu^{III}(oep)$_2$.[5] Gadolinium, the second exception, has an $^8S_{7/2}$ ground state and a long spin lattice relaxation time. It exhibits an observable EPR signal at room temperature which is probably due to the metal. The only energy levels of Gd(III) accessible to EPR are those of the ground state multiplet $^8S_{7/2}$. The nearest excited state multiplet, $^7P_{7/2}$, is separated from the ground states by energies in the ultraviolet range. This ground state multiplet, $^8S_{7/2}$, may be split by the crystal field at zero magnetic field (ZFS), and this seems to be the case. The different double-deckers Gd^{III}(oep)$_2$, Gd^{III}H(tpp)$_2$, and the Gd^{III}(tpp)(acac) present slightly different EPR spectra (see also Supporting Information), probably due to the different ligands. Upon oxidation, the EPR spectrum of Gd(III) heteroleptic complex consists of an intense signal, indicative of the π-cation radical formed.

UV−Visible Spectroscopy. UV−visible data that have been reported in the literature for lanthanide,[21−33] actinide,[9,18,34,35] Zr(IV),[12,36,37] and Hf(IV)[12,37] porphyrinic sandwich complexes make it clear that the strong $\pi-\pi$ interaction between the two macrocycles results in the appearance of new optical features. The origin of these features is discussed in terms of "excitonic interactions", which are probably responsible for the broad and blue-shifted Soret band of the bis-porphyrinates, as well as in terms of ring-to-ring charge transfer transitions or ring-to-metal charge transfer phenomena (RRCT and RMCT), respectively.[8,9,19,35] The spectra of the title compounds were measured both in CH_2Cl_2 (in which solvent form **A** of equilibrium 1 is present) and in DMF (in which form **B** is dominant). The spectral features in CH_2Cl_2[31] (Figure 2) exhibit striking differences compared to the corresponding complexes of actinide(IV),[35] Zr(IV), Hf(IV),[12,37] and Ce(IV).[19,20] These differences are due to the different oxidation states of the metal ions, +4 for actinide and +3 for lanthanide derivatives, which cause both porphyrinic ligands to appear as dianions in the case of M^{4+} while one as monoanion and the other as dianion in the case of M^{3+}. In the latter case, the H^+ resides on one of the porphyrin rings, as in the case of the lanthanide phthalocyanine sandwich-like derivatives. On the other hand, the UV−visible data in DMF[31] present features similar to those of the corresponding Ac(IV) derivatives (Figure 3). Thus, the protonated heteroleptic and homoleptic lanthanide sandwiches reported here could be represented by the following formulas: Ln^{III}H(porph)(porph′), Ln^{III}(porphH)(porph′), or Ln^{III}(porph)(porph′H), where porph = or ≠ porph′ and the porphyrin macrocycle which possesses the proton is a monoanion [porph^{-1}]H and the other one is a dianion [porph^{-2}]. The deprotonated complexes could be

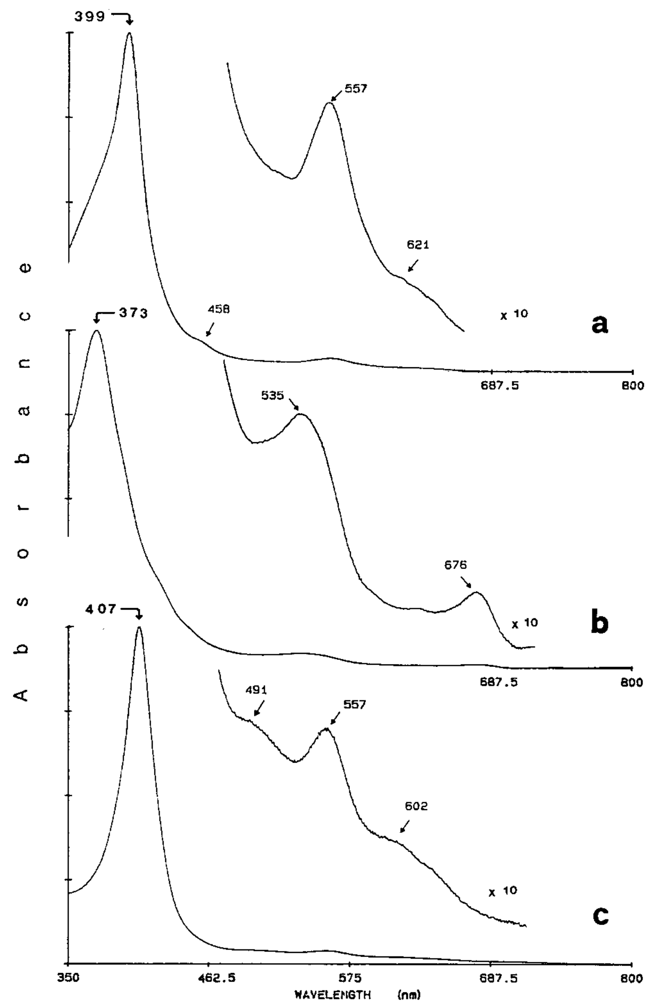

Figure 2. UV−visible spectra of (a) Gd^{III}H(oep)(tpp), (b) Gd^{III}(oep)$_2$, and (c) Gd^{III}H(tpp)$_2$ double-deckers in CH_2Cl_2.

presented by the formula [Ln^{III}(porph)(porph′)]$^-$[X]$^+$. It is noteworthy that none of the title compounds exhibit the characteristic near-infrared absorption band of a π-cation sandwich-like complex in the region of 900−1200 nm. This finding leads to the conclusion that the purification procedure described herein yields only the neutral symmetrical tpp and asymmetrical double-deckers, free of chemically generated π-radicals, and that deprotonation of the complexes under the experimental conditions described above (basic solvents) does not result in any π-cation complex.

Homoleptic Double-Deckers. The optical data of Ln^{III}H(tpp)$_2$ in CH_2Cl_2 are presented in Table 3. All complexes exhibit a single broad Soret band which is significantly blue-shifted with respect to the corresponding monoporphyrinates. The Soret band maximum varies from 409 nm in [Nd^{III}H(tpp)$_2$] to 404 nm in [Lu^{III}H(tpp)$_2$]. Thus, a small shift to the blue region is observed for the homoleptic tpp complexes as the ionic radium of the metal ion is reduced (lanthanide contraction). This observation is in agreement with a similar shift observed for some cofacial and strongly coupled porphyrinic sandwiches upon diminution of the interporphyrin distance and it is probably due to the increase of the excitonic interactions.[2,4] No corresponding shift along the series is observed for the three annex bands in the regions around 490, 555, and 610 nm.

The UV−visible data in DMF (Table 4) where form **B** is dominant display significant differences. They exhibit a single Soret band which is also blue-shifted along the series, but five

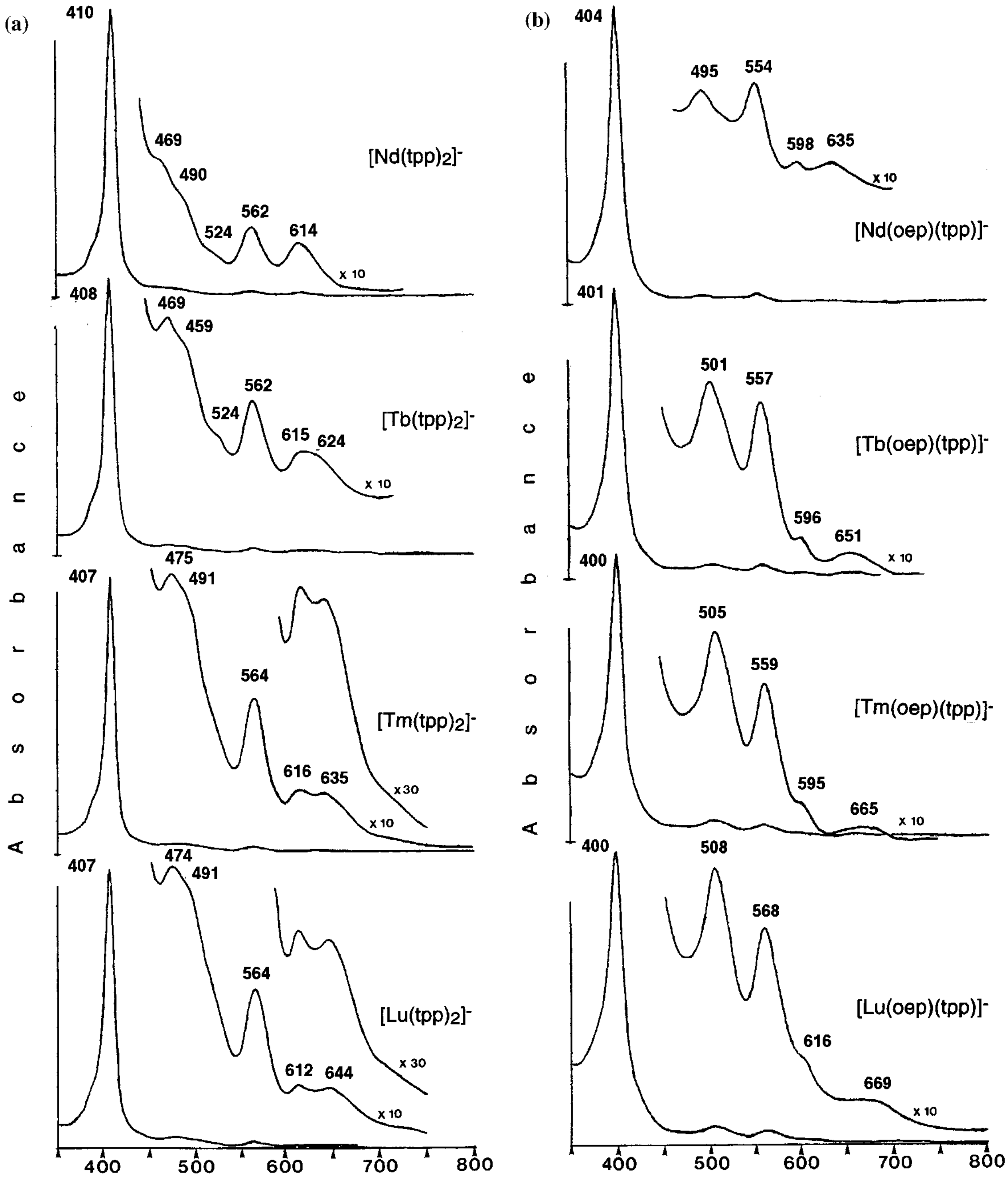

Figure 3. UV−visible spectra of few (a) homoleptic $[Ln^{III}(tpp)_2]^-$ and the corresponding (b) heteroleptic $[Ln^{III}(oep)(tpp)]^-$ double-deckers in DMF.

bands appear in the region 460−650 nm. Among the latter, one at 470 nm and a second at 615 nm for the complexes from Nd to Gd derivatives. The low-energy band at ∼615 nm is the $Q(0,0)$. For the heavy lanthanide ions (Tb to Lu) this band splits into two components, one at ∼615 nm and the other at ∼645 nm. It is strongly believed that the origin of the latter band corresponds to Q' while the the high-energy annex band at ∼470 nm corresponds to Q'', since they appear in the same regions for the cases of Ac(IV)[35] and other M^{IV} sandwich-like complexes.[12,36,37] A significant red-shift is observed for both Q'' and Q'. The latter shifts from 624 nm in the case of $[Tb^{III}(tpp)_2]^-$ to 644 nm in the case of $[Lu^{III}(tpp)_2]^-$ (Figure 3a). A similar shift, due to the different ionic radii of the central metals, has been observed for the Ac(IV),[35] Zr(IV),[12,36,37] and Hf(IV)[12,37] complexes and has been attributed to the increased interaction between the two macrocycles. Their origin could be discussed in terms of charge transfer transitions, between the two porphyrin rings [ring-to-ring charge transfer, RRCT] or between the metal and the porphyrin ring [ring-to-metal charge transfer, RMCT], rather than to excitonic interaction between the two tetrapyrrole ligands.[19,35]

Moreover, two ill-defined bands of medium and low intensity are observed in the region between 485 and 530 nm and do not seem to be affected by the change of the metal ion along the lanthanide series. Their origin is not clear to us.

Heteroleptic Double-Deckers. The optical data for $Ln^{III}H$-(oep)(tpp) taken in CH_2Cl_2 are presented in Table 5. All the complexes exhibit a single Soret band at around 400 nm. A small blue shift is also observed from Nd(III) to Lu(III) (see Table 5) for the same reason as in the homoleptic case. This band is blue-shifted by approximately 10 nm compared to the $Ln^{III}H(tpp)_2$ and red-shifted 20 nm compared to the $Ln^{III}(oep)\}_2$[4] complexes. In the region of the annex bands, in addition to the major band at 555−560 nm, a new one appears at around 460

Table 3. UV−Visible Data for Homoleptic $Ln^{III}H(tpp)_2$, Where Ln = Nd, ..., Lu (except Pm) in CH_2Cl_2 [λ/nm (log ϵ dm^{-3} mol^{-1} cm^{-1})]

Ln	*B* band	*Q* bands		
Nd	409	492	557	605
	(5.42)	(3.84)	(3.92)	(3.59)
Sm	409	492	556	604
	(5.41)	(3.84)	(3.92)	(3.59)
Eu	408	491	556	605
	(5.42)	(3.88)	(3.93)	(3.59)
Gd	407	491	557	602
	(5.41)	(3.93)	(3.94)	(3.59)
Tb	406	494	554	602
	(5.42)	(3.94)	(3.93)	(3.60)
Dy	407	491	558	602
	(5.41)	(3.94)	(3.90)	(3.58)
Ho	407	490	558	605
	(5.43)	(3.90)	(3.89)	(3.55)
Er	407	490	559	605
	(5.43)	(3.91)	(3.91)	(3.48)
Tm	405	492	558	605
	(5.41)	(3.91)	(3.88)	(3.53)
Yb	405	491	556	609
	(5.42)	(3.92)	(3.87)	(3.50)
Lu	404	493	555	616
	(5.43)	(3.92)	(3.86)	(3.51)

Table 4. UV−Visible Data for Homoleptic $[Ln^{III}(tpp)_2]^-$, Where Ln = Nd, ..., Lu (except Pm) in DMF [λ/nm (log ϵ dm^{-3} mol^{-1} cm^{-1})]

Ln	*B* band	*Q* bands					
Nd	410	469	490	524	562	614	
	(5.68)	(4.13)	(4.00)	(3.83)	(3.89)	(3.61)	
Sm	410	469	490	524	562	614	
	(5.67)	(4.14)	(4.04)	(3.80)	(3.89)	(2.79)	
Eu	409	467	491	524	561	613	
	(5.67)	(4.16)	(4.08)	(3.80)	(3.90)	(3.48)	
Gd	408	470	491	524	561	616	
	(5.66)	(4.14)	(4.08)	(3.79)	(3.89)	(3.48)	
Tb	408	469	489	524	562	615	624
	(5.64)	(4.10)	(4.07)	(3.77)	(3.85)	(3.46)	(3.42)
Dy	408	471	491	524	562	618	630
	(5.65)	(4.11)	(4.06)	(3.78)	(3.85)	(3.47)	(3.42)
Ho	407	473	492	523	563	620	635
	(5.66)	(4.12)	(4.10)	(3.79)	(3.90)	(3.48)	(3.45)
Er	407	474	492	524	563	623	638
	(5.66)	(4.12)	(4.11)	(3.79)	(3.86)	(3.49)	(3.44)
Tm	407	475	491	524	564	616	635
	(5.67)	(4.14)	(4.10)	(3.80)	(3.88)	(3.48)	(3.46)
Yb	407	473	491	524	562	612	640
	(5.67)	(4.15)	(4.12)	(3.80)	(3.90)	(3.48)	(3.46)
Lu	407	474	491	522	564	612	644
	(5.67)	(4.15)	(4.12)	(3.80)	(3.90)	(3.49)	(3.45)

nm. The origin of this band is difficult to elucidate. However, it could be compared with the analogous absorption Q'' band of $Ln^{III}H(tpp)_2$, which was observed around 490 nm (see Table 3), and with other Ac^{IV}(oep)(tpp) derivatives.[35] Moreover, the above absorption band characteristic for the heteroleptic lanthanide porphyrin complexes is systematically observed, and we noted here that such band has not been reported for the already described La(III)[23] and Eu(III)[14] heteroleptic double-deckers. In the region of the annex bands, no absorption band was observed in the region of 600−750 nm, in contrast to $Ln^{III}(oep)_2$ complexes, which exhibit a characteristic band at 680 nm.[4]

The UV−visible data of the heteroleptics in DMF, where form **B** is dominant, are presented in Table 6, and a few spectra are illustrated in Figure 3b. These spectra again have different features compared to those of the protonated complexes and furthermore exhibit significant differences compared to the analogous symmetrical complexes $[Ln^{III}(tpp)_2]^-$ in DMF (Tables 4 and 6 and Figure 3a,b). The Soret band again displays a small blue shift along the series from 400 to 404 nm. In the region of the annex bands we observe four absorptions. From these, the highest and lowest energy bands (500 and 650 nm) display a red shift along the series and by analogy to the homoleptic complexes we assign them to Q'' and Q', respectively. Furthermore, these two bands are also red-shifted with respect to the corresponding *Q* bands of homoleptic complexes. This could be explained on the reasonable assumption that one oep and one tpp ligand pack more efficiently around the central metal than two tpp ligands.

Table 5. UV−Visible Data for Heteroleptic $Ln^{III}H$(tpp)(oep), Where Ln = Nd, ..., Lu (except Pm) in CH_2Cl_2 [λ/nm (log ϵ dm^{-3} mol^{-1} cm^{-1})]

Ln	*B* band	*Q* bands		
Nd	401	452	555	611
	(5.22)	(4.23)	(3.90)	(3.72)
Sm	400	453	556	613
	(5.23)	(4.22)	(3.90)	(3.70)
Eu	400	455	556	621
	(5.20)	(4.18)	(3.88)	(3.69)
Gd	399	458	557	621
	(5.21)	(4.20)	(3.85)	(3.68)
Tb	398	456	556	627
	(5.20)	(4.16)	(3.80)	(3.67)
Dy	398	457	556	630
	(5.17)	(4.14)	(3.78)	(3.67)
Ho	397	457	559	636
	(5.18)	(4.15)	(3.80)	(3.67)
Er	397	457	558	639
	(5.22)	(4.20)	(3.88)	(3.69)
Tm	396	456	558	641
	(5.19)	(4.17)	(3.85)	(3.68)
Yb	396	457	560	625
	(5.18)	(4.14)	(3.80)	(3.67)
Lu	396	457	558	629
	(5.17)	(4.13)	(3.79)	(3.65)

Table 6. UV−Visible Data for Heteroleptic $[Ln^{III}(oep)(tpp)]^-$, Where Ln = Nd, ..., Lu (except Pm) in DMF [λ/nm (log ϵ dm^{-3} mol^{-1} cm^{-1})]

Ln	*B* band	*Q* bands			
Nd	404	495	554	598	635
	(5.45)	(3.90)	(4.04)	(3.61)	(3.42)
Sm	403	498	556	598	641
	(5.45)	(3.95)	(4.03)	(3.62)	(3.41)
Eu	402	499	557	598	645
	(5.45)	(3.97)	(4.03)	(3.62)	(3.41)
Gd	402	499	557	596	647
	(5.44)	(4.04)	(4.03)	(3.61)	(3.41)
Tb	401	501	557	596	651
	(5.45)	(4.05)	(4.02)	(3.61)	(3.40)
Dy	400	503	558	596	657
	(5.44)	(4.06)	(4.03)	(3.60)	(3.39)
Ho	400	504	558	596	659
	(5.44)	(4.08)	(4.01)	(3.60)	(3.41)
Er	400	503	558	596	663
	(5.44)	(4.08)	(4.02)	(3.60)	(3.46)
Tm	400	505	559	595	665
	(5.43)	(4.04)	(3.98)	(3.55)	(3.33)
Yb	400	505	559	595	666
	(5.43)	(4.02)	(3.97)	(3.55)	(3.34)
Lu	400	506	568	616	669
	(5.40)	(3.96)	(3.66)	(3.36)	(3.20)

Finally, it is quite clear that the optical spectra of the mixed oep-tpp double-deckers display the characteristic features that are closer to those of the symmetrical tpp derivatives than to those of the oep analogs, indicating a stronger involvement of the tpp macrocycle. This is confirmed both by the IR and the electrochemical studies presented below.

Table 7. UV−Visible Data for Gd Oxidized Heteroleptic and Homoleptic Double-Deckers in CH_2Cl_2 [λ/nm (log ϵ dm^{-3} mol^{-1} cm^{-1})]

	B band	*Q* bands	NIR
[Gd(oep)(tpp)]$^\bullet$	359 (4.98)	596 (4.02)	980 (4.07)
[Gd^{III}(tpp)$_2$]$^\bullet$	376 (5.06)	591 (4.02)	1020 [1015][a] (4.15)

[a] Reference 11.

Oxidized Double-Deckers. The oxidation of the Gd(III) double-deckers leads to the non-protonated form of the complexes. The UV−visible spectra of these oxidized, homo- and heteroleptic complexes (Table 7) consist of a single Soret band at about 360 nm (heteroleptic) and 376 nm (homoleptic) and only one annex band between 589 and 597 nm, close to the λ_{max} of the absorption band observed in the case of the electrogenerated [Pr^{III}(oep)$_2$]$^{+\bullet}$$ClO_4^-$.[4] As in the case of the precursors discussed above, the Soret band appears at higher energy wavelengths in the heteroleptic complexes than in the corresponding homoleptic derivatives, indicating larger excitonic coupling in the former complexes. The electron hole of the oxidized species is confirmed by the NIR absorption band. For the studied case of Gd(III), we observe the NIR absorption band at 980 nm for the hetero- and at 1020 nm for the homoleptic derivatives (Table 7).

FT-IR Spectroscopy. The IR data of the neutral heteroleptic complexes display the characteristic bands of both tpp and oep. Of more interest are the IR spectra of the oxidized species which were studied in an attempt to locate the electron hole. Three complexes were chosen: [Gd^{III}(tpp)$_2$]$^\bullet$, [Gd^{III}(oep)(tpp)]$^\bullet$, and Gd^{III}(oep)$_2$ (the latter is considered as a one hole species,[4] NIR band ∼1250 nm). Characteristic IR bands for tpp π-radicals were observed between 1270 and 1295 cm^{-1}, where similar bands for oep π-radicals, detected between 1520 and 1570 cm^{-1}.[44,45] Indeed, for the two Gd(III) π-radicals, Gd(oep)$_2$ and [Gd(tpp)$_2$]$^\bullet$, respectively, IR characteristic bands were observed in the aforementioned region. More specifically, bands at 1562 and 1528 cm^{-1} were observed for homoleptic oep (Figure 4a), while for the tpp analog, strong bands were observed at 1226 and 1268 cm^{-1} (Figure 4c). The dramatic enhancement of the above peaks intensity is probably characteristic of oxidizing tpp moieties in porphyrin double-deckers. The IR spectrum of [Gd^{III}-(oep)(tpp)]$^\bullet$ contains very strong bands in the tpp region and only very weak bands in the oep region (Figure 4b). We take this as strong evidence that the hole primarily resides on the tpp macrocycle. This is in agreement with the above-mentioned UV−visible study and the electrochemical study that follows. It is, however, in contrast to the recently published work on Ac(IV) double-deckers where the electron hole resides on the oep macrocycle.[34]

Electrochemistry. The electrochemical behavior of the title complexes was investigated in two solvents in analogy with their UV−visible investigation. THF was used instead of DMF, due to its broader redox limits. For an indicative comparison, the redox properties of three precursor lanthanide monoporphyrinates were also studied under the same experimental conditions: [Sm^{III}(tpp)acac, −1.81, −1.39, −0.72, 0.95, and 1.27 V; Eu^{III}(tpp)acac, −1.80, −1.37, −0.76, 0.99, and 1.30 V; Gd^{III}(tpp)acac, −1.88, −1.31, −0.81, 1.03, and 1.26 V]. Values of $E_{1/2}$ were obtained for the dominant forms **A** (in CH_2-

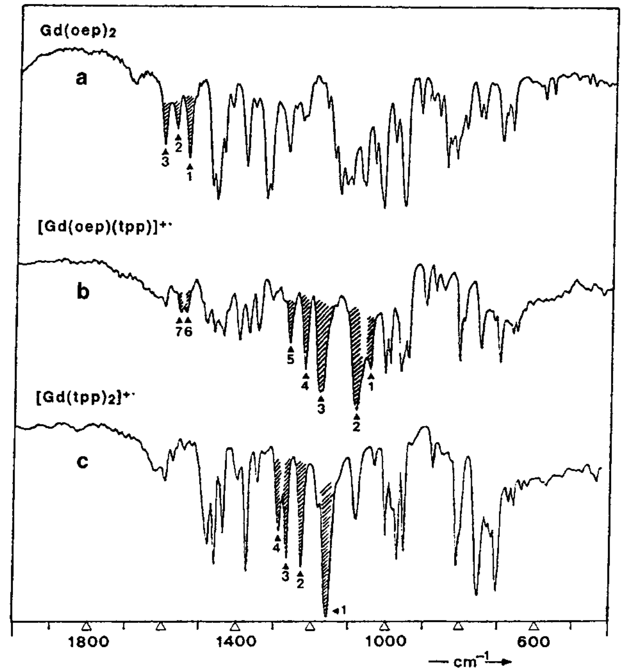

Figure 4. FT-IR data for (a) Gd^{III}(oep)$_2$, (b) [Gd^{III}(oep)(tpp)]$^\bullet$, and (c) [Gd^{III}(tpp)$_2$]$^\bullet$.

Cl_2) and **B** (in THF) (see eq 1) for all the title complexes.[46] In order to confirm the nature of the electron process in both solvents, representative cyclic and linear voltammetry electrochemical experiments (not shown) were carried out for the first two electrooxidations. The data indicate that the above-mentioned process involved one-electron oxidation (electrochemical oxidation), with a smaller $E_{1/2}$(1st ox) − $E_{1/2}$(1st red) difference in the case of THF (0.25 V) than in CH_2Cl_2 (0.4 V). These data are summarized in Tables 8 and 9 for the homoleptic and in Tables 10 and 11 for the heteroleptic complexes.

In CH_2Cl_2, only the oxidation process was observed for both homo- and heteroleptic complexes. In THF the heteroleptic complexes undergo three oxidations and one reduction while the homoleptic ones undergo two oxidations and two reductions within the limits of the solvent. All the processes correspond to one-electron transfer exhibiting values $E_{pc} - E_{pa} = 60 \pm 5$ mV. For these processes the peak current is proportional to $\upsilon^{1/2}$. The overall chemical and electrochemical reactions in both solvents are presented in Figure 5. All the observed electrode reactions correspond to the electrochemical processes centered on the porphyrin macrocycles. In order to discriminate the waves that correspond to forms **A** and **B** of the complexes, cyclic and linear voltammetry studies were carried out in CH_2Cl_2 solution, before and after the addition of a strong base, Et_3N.[33] Under the latter condition we shift equilibrium 1 to the deprotonated form (**B**) and thus all the electrochemical processes observed are due to the deprotonated complex.[33] According to our results, the deprotonated complexes oxidized more easily (see E_5 in Tables 8 and 10) than the corresponding protonated form (which undergo two quasi-reversible oxidations, denoted as E_7 and E_8). The electrochemical reactions which yield the singly and doubly oxidized protonated species, [Ln^{III}(porph)(porph)′]$^{n+}$ (where porph = or ≠ porph′ and n = 1, 2), are also quasi-reversible. Following oxidation of the complexes, the proton becomes more

(44) Scholtz, W. F.; Reed, C. A.; Lee, Y. J.; Scheidt, W. R.; Lang, G. *J. Am. Chem. Soc.* **1982**, *104*, 6791−6793.
(45) Shimomura, E. T.; Phillippi, M. A.; Goff, H. M. *J. Am. Chem. Soc.* **1981**, *103*, 6778−6780.

(46) We should clarify at this point that in UV−visible only form **A** is present in CH_2Cl_2 but in electrochemistry in the same solvent we observe a time dependent equilibrium between forms **A** and **B** due the presence of the support electrolyte; see also ref 33.

Table 8. Half-Wave Redox Potentials (V vs SCE) of Homoleptic tpp Ln Double-Deckers (Where Ln = Nd, ..., Lu, except Pm) in CH_2Cl_2

Ln	E_5	E_6	ΔE_3 ($E_5 - E_6$)	E_7[a]	E_8[b]	ΔE_4 ($E_7 - E_8$)	E_9	ΔE_5 ($E_6 - E_9$)	E_{10}	ΔE_6 ($E_9 - E_{10}$)
Nd	0.14	0.49	0.35	0.65	0.96	0.31	1.26	0.77	1.54	0.28
Sm	0.12	0.46	0.34	0.64	0.97	0.33	1.27	0.81	1.57	0.30
Eu	0.14	0.45	0.31	0.63	0.97	0.34	1.29	0.84	1.59	0.30
Gd	0.11	0.44	0.33	0.62	0.92	0.30	1.28	0.84	1.60	0.32
Tb	0.09	0.41	0.32	0.61	0.92	0.31	1.27	0.86	1.60	0.33
Dy	0.07	0.39	0.32	0.60	0.91	0.31	1.27	0.88	1.62	0.33
Ho	0.06	0.40	0.34	0.61	0.88	0.27	1.27	0.87	1.63	0.36
Er	0.06	0.38	0.32	0.59	0.88	0.29	1.27	0.89	1.63	0.36
Tm	0.05	0.37	0.32	0.59	0.87	0.28	1.27	0.90	1.64	0.37
Yb	0.06	0.38	0.32	0.59	0.86	0.27	1.27	0.89	1.65	0.38
Lu	0.03	0.36	0.33	0.58	0.83	0.25	1.27	0.89	1.63	0.38

[a] Quasi-reversible process, $E_{1/2}$ of first oxidation of protonated species. [b] Quasi-reversible process, $E_{1/2}$ of second oxidation of protonated species.

Table 9. Half-Wave Redox Potentials (V vs SCE) of Homoleptic tpp Ln Double-Deckers (Where Ln = Nd, ..., Lu, except Pm) in THF

Ln	ionic radius (pm)[a]	reduction			oxidation			HOMO−LUMO gap (V)
		E_1	E_2	ΔE_1 ($E_1 - E_2$)	E_3	E_4	ΔE_2 ($E_3 - E_4$)	
Nd	*112*	−1.87	−1.48	0.39	0.37	0.79	0.42	1.85
Sm	*109*	−1.88	−1.49	0.39	0.35	0.75	0.40	1.84
Eu	*107*	−1.94	−1.52	0.42	0.33	0.72	0.39	1.85
Gd	*106*	−1.89	−1.50	0.39	0.35	0.76	0.41	1.85
Tb	*104*	−1.87	−1.48	0.39	0.35	0.76	0.42	1.83
Dy	*103*	−1.87	−1.49	0.38	0.31	0.75	0.44	1.80
Ho	*102*	−1.89	−1.50	0.39	0.31	0.72	0.41	1.81
Er	*100*	−1.86	−1.49	0.37	0.33	0.72	0.40	1.82
Tm	*99*	−1.89	−1.49	0.40	0.31	0.73	0.42	1.80
Yb	*98*	−1.91	−1.49	0.42	0.31	0.72	0.42	1.80
Lu	*97*	−1.86	−1.49	0.37	0.31	0.75	0.44	1.80

[a] Reference 51.

Table 10. Half-Wave Redox Potentials (V vs SCE) of Heteroleptic Ln Double-Deckers (Where Ln = Nd, ..., Lu, except Pm) in CH_2Cl_2

Ln	E_5	E_6	ΔE_3 ($E_5 - E_6$)	E_7[a]	E_8[b]	ΔE_4 ($E_7 - E_8$)	E_9	ΔE_5 ($E_6 - E_9$)	E_{10}	ΔE_6 ($E_9 - E_{10}$)
Nd	−0.03	0.39	0.42	0.55	0.85	0.30	1.17	0.78	1.47	0.30
Sm	−0.06	0.38	0.44	0.52	0.86	0.34	1.17	0.79	1.50	0.33
Eu	−0.08	0.36	0.44	0.50	0.88	0.38	1.17	0.81	1.51	0.34
Gd	−0.11	0.33	0.44	0.46	0.88	0.32	1.16	0.83	1.54	0.38
Tb	−0.09	0.34	0.43	0.49	0.81	0.32	1.19	0.85	1.54	0.35
Dy	−0.11	0.33	0.44	0.49	0.84	0.35	1.18	0.85	1.55	0.37
Ho	−0.14	0.30	0.44	0.47	0.80	0.33	1.18	0.88	1.55	0.37
Er	−0.15	0.29	0.44	0.45	0.79	0.32	1.17	0.88	1.54	0.37
Tm	−0.13	0.29	0.42	0.47	0.80	0.33	1.19	0.90	1.57	0.38
Yb	−0.16	0.28	0.44	0.46	0.79	0.33	1.20	0.92	1.57	0.37
Lu	−0.16	0.27	0.43	0.45	0.78	0.33	1.20	0.93	1.58	0.38

[a] Quasi-reversible process, $E_{1/2}$ of first oxidation of protonated species. [b] Quasi-reversible process, $E_{1/2}$ of second oxidation of protonated species.

Table 11. Half-Wave Potentials (V vs SCE) for Oxidation and Reduction of Heteroleptic Ln Double-Deckers (Where Ln = Nd, ..., Lu, except Pm) in THF

Ln	ionic radius (pm)[a]	reduction			oxidation			HOMO−LUMO gap (V)
		E_1	E_2	ΔE_1 ($E_2 - E_3$)	E_3	E_4	ΔE_2 ($E_3 - E_4$)	
Nd	*112*	−1.51	0.23	0.40	0.63	1.29	0.66	1.74
Sm	*109*	−1.51	0.22	0.39	0.61	1.29	0.68	1.73
Eu	*107*	−1.55	0.19	0.39	0.58	1.29	0.71	1.74
Gd	*106*	−1.57	0.17	0.40	0.57	1.26	0.69	1.74
Tb	*104*	−1.60	0.15	0.40	0.55	1.30	0.75	1.75
Dy	*103*	−1.61	0.10	0.42	0.52	1.28	0.76	1.71
Ho	*102*	−1.61	0.08	0.44	0.52	1.28	0.76	1.69
Er	*100*	−1.60	0.06	0.47	0.53	1.30	0.77	1.66
Tm	*98*	−1.60	0.07	0.45	0.52	1.31	0.79	1.67
Yb	*98*	−1.61	0.06	0.46	0.52	1.31	0.79	1.67
Lu	*97*	−1.62	0.06	0.45	0.51	1.32	0.81	1.68

[a] Reference 51.

acidic and deprotonation (chemical reaction) follows the electron abstraction. The doubly oxidized protonated species are more active (quasi-reversible or irreversible electron process) than the singly oxidized ones and this is probably why we do not observe a third oxidation. Examples of the cyclic voltammograms for the two forms $Er^{III}H(tpp)_2$, $[Er^{III}(tpp)_2]^-$ and $Er^{III}H(tpp)(oep)$, $[Er^{III}(tpp)(oep)]^-$ in CH_2Cl_2 are given in Figure 6, while $[Er^{III}(tpp)(oep)]^-$ in THF is given in Figure 7.

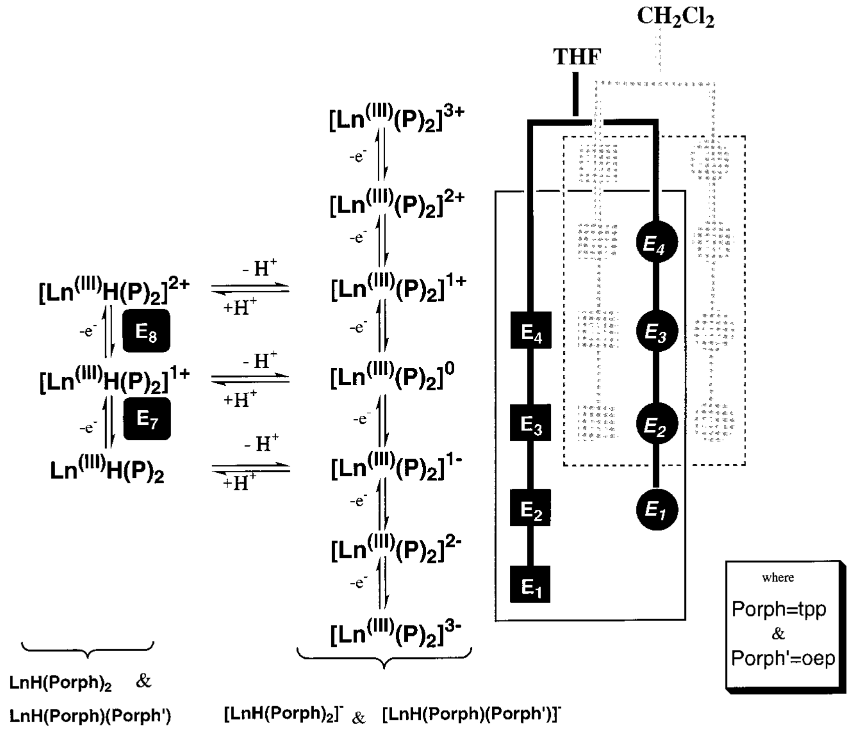

Figure 5. General scheme of chemical/electrochemical processes.

In summary, the heteroleptic complexes oxidized more easily than the corresponding homoleptic in both solvents, CH_2Cl_2 and THF, but reduced harder in THF. Comparison of the electrochemical data of the title compounds with the data reported for $Ln^{III}(oep)_2$ confirms that the former oxidized harder but reduced considerably easier than the latter.

The HOMO−LUMO gap of these double-deckers, which could be expressed by the half-wave potential $E_{1/2}$(1st ox) − $E_{1/2}$(1st red), is smaller than the HOMO−LUMO gap of the corresponding monoporphyrinate complexes and this is illustrated in Figure 8 for the case of Sm(III). The difference $E_{1/2}$(1st ox) − $E_{1/2}$(1st red) decreases from 2.16 V for Sm^{III}(tpp)acac, to 1.83 V in the homoleptic, $Sm^{III}(oep)_2$ and $[Sm^{III}(tpp)_2]^-$ complexes and, drops finally to 1.73 V in the heteroleptic complex $[Sm^{III}(oep)(tpp)]^-$. This HOMO−LUMO gap for heteroleptic complexes varies from 1.73 V (Nd complex) to 1.68 V (Lu complex). As it is illustrated at Figure 9, $E_{1/2}$(1st red), $E_{1/2}$(1st ox), and $E_{1/2}$(2nd ox) for $[Sm^{III}H(oep)(tpp)]^-$ are closer to the corresponding $E_{1/2}$ values of $[Sm^{III}H(tpp)_2]^-$ than for Sm^{III}-$(oep)_2$. This observation is true for all the title complexes in CH_2Cl_2 and THF. Thus, the electron transfer process in which an electron is donated to or abstracted from porphyrinic orbitals involves orbitals of mainly tpp character. This is in agreement with the already mentioned IR conclusion. This result is contrary to the heteroleptic M(IV) complexes for which electrochemical as well as resonance Raman studies indicate a rather equal contribution of oep and tpp orbitals for U(IV) and Th(IV)[34] and a mainly oep contribution from Ce(IV).[7,16,21,26]

Magnetic Susceptibility Measurements. Magnetic susceptibility data for $Ln^{III}H(oep)(tpp)$ from 300 to 5 K are in good agreement with those expected for trivalent lanthanides both with regard to the room temperature[47] magnetic moment as well as their temperature dependance.[48] If for example we consider the $Gd^{III}H(oep)(tpp)$ complex, it obeys the Curie−Weiss law (Figure 10). The linear regression of the curve $1/\chi$ versus T gives the equation: $\chi(T - 0.58) = 7.604$. However, the two complexes of Sm and Eu did not obey the Curie law. Between 5 and 300 K, we observe a large temperature dependence of the magnetic moment (Table 12). This phenomenon was explained by comparing the multiplet width to kT; for the above-mentioned complexes (Sm, Eu) these two terms are comparable and a Van Vleck type equation (which includes a g factor and the Nα contribution) can be used to simulate quite satisfactorily the complicated temperature dependence of the moments of these two trivalent ions.[49]

X-ray Structure. The molecular structure of the complex $Gd^{III}H(oep)(tpp)$ was determined by X-ray structure analysis at room temperature (Figure 11). The structure will be discussed in comparison with Sm(III) analog. The asymmetric unit contains one discrete double-decker molecule and one dichloromethane molecule. The coordination polyhedron of Gd(III), as in the case of Sm(III), is a square antiprism where the two porphyrin rings are rotated by an angle of 45.02° (mean value). The mean bond length of Gd−N(tpp) is 2.524 Å and that for Gd−N(oep) is 2.551 Å. These values are slightly shorter than in $Sm^{III}H(oep)(tpp)$ (mean values Sm−N(tpp) = 2.538 Å, and for Sm−N(oep) = 2.565 Å), in agreement with the shorter ionic radius of Gd(III) compared to Sm(III). Gadolinium lies 1.450 and 1.495 Å off the mean plane defined by the $N_1N_2N_3N_4$ and $N_5N_6N_7N_8$ atoms of the tpp and oep ring, respectively. Thus the separation of two N_4 planes is 2.945 Å while for the slightly larger Sm(III) ion it was found to be 2.986 Å. The two N_4 mean planes of the macrocycles are almost parallel, having an angle of 1.29°. The distance δ_{CN} of the $C_{20}N_4$ mean plane and the N_4 plane, which is the measure of the doming, is 0.243 Å for the tpp and 0.313 Å for the oep, indicating that the oep ring is more deformed. Thus, the two mean planes of the core atoms, $C_{20}N_4$, of the individual macrocycles are 3.501 Å (2.945 + 0.243 +

(47) Vickery, R. C. *Chemistry of Lanthanons*; Butterworths Scientific Publications: London, 1953.

(48) Foex, G. Constantes selectionnees Diamagnetisme et Paramagnetism. In *Tables de constantes et données numériques*; Masson et Cie: Paris, 1957; Vol. 7.

(49) Earnshaw, A. *Introduction to Magnetochemistry*; Academic Press: London, 1968.

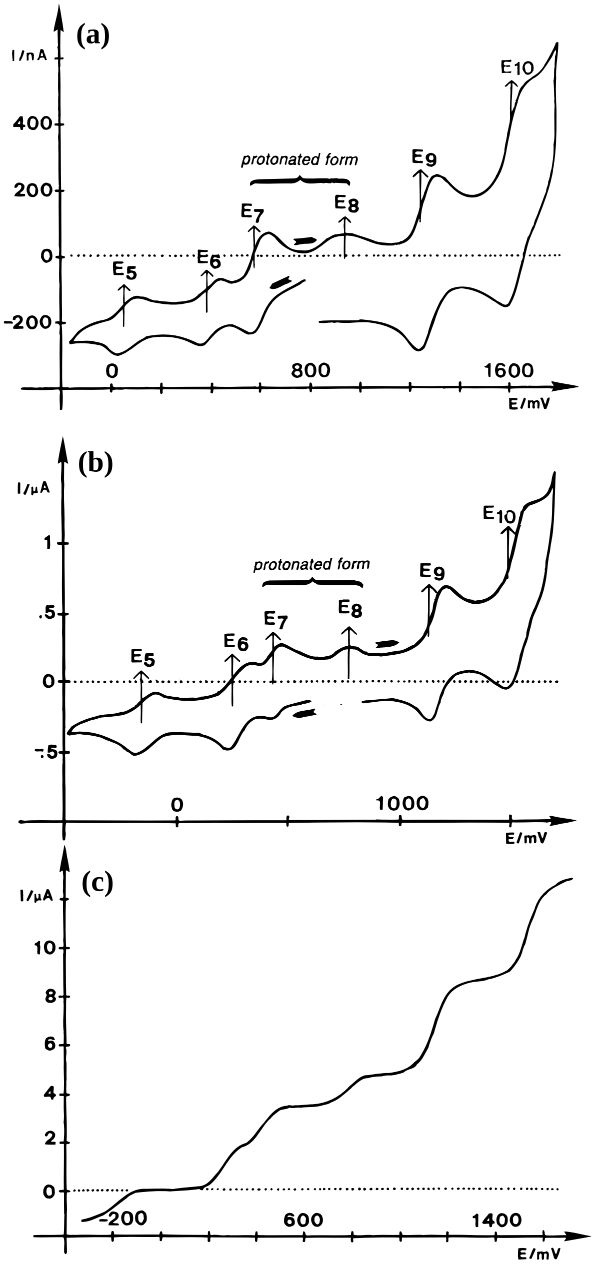

Figure 6. (a) Cyclic voltammogram of $Er^{III}H(tpp)_2$, $[Er^{III}(tpp)_2]^-$ forms; (b) cyclic voltammogram of $Er^{III}H(oep)(tpp)$, $[Er^{III}(oep)(tpp)]^-$ forms; and (c) linear voltammetry of $Er^{III}H(oep)(tpp)$, $[Er^{III}(oep)(tpp)]^-$ forms, in 0.1 M CH_2Cl_2/NBu_4PF_6 (scan rate 0.1 V s^{-1} V vs SCE, 21 °C).

0.313) apart. The δ_{CN} values found for the analogous complex $Sm^{III}H(oep)(tpp)$ were 0.233 Å for the tpp and 0.316 for the oep. The mean displacements of the core atoms, $C_{20}N_4$, from their plane are 0.127 Å (tpp) and 0.169 Å (oep) for the $Gd^{III}H$(oep)(tpp) complex and 0.123 Å (tpp) and 0.175 Å (oep) for $Sm^{III}H$(oep)(tpp). The average of the dihedral angles ω of the individual pyrrole rings with respect to the corresponding $C_{20}N_4$ mean plane are as follows: (tpp) 11.12°; (oep) 14.31°. These values corroborate the stronger doming of the oep ring with respect to the tpp ring also found in the Sm(III) complex [ω values 10.68° (tpp), 14.69° (oep)]. The four pyrrole rings form the following dihedral angles with the $N_1N_2N_3N_4$ plane of the tpp ring: $C_1C_2C_3C_4N_1$, 14.96°; $C_6C_7C_8C_9N_2$, 7.90°; $C_{11}C_{12}C_{13}C_{14}N_3$, 12.61°; and $C_{16}C_{17}C_{18}C_{19}N_4$, 9.04°. For the oep ring these values are $C_{45}C_{46}C_{47}C_{48}N_5$, 8.28°; $C_{50}C_{51}C_{52}C_{53}N_6$, 13.72°; $C_{55}C_{56}C_{57}C_{58}N_7$, 16.63°; and $C_{60}C_{61}C_{62}C_{63}N_8$, 18.63°. The individual pyrrole rings are planar within experimental error. The phenyl rings of the tpp form the following dihedral angles with the $C_{20}N_4$ plane: $C_{21}-C_{26}$, 80.98°; $C_{27}-C_{32}$, 62.89°; $C_{33}-C_{38}$, 77.403°; and $C_{39}-C_{44}$, 83.86°.

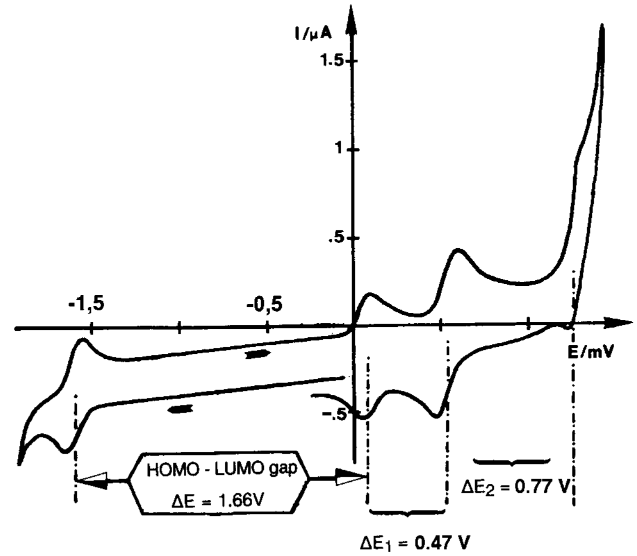

Figure 7. Cyclic voltammogram of $[Er^{III}(oep)(tpp)]^-$, in 0.1 M THF/NBu_4PF_6 (scan rate 0.1 V s^{-1} V vs SCE, 21 °C).

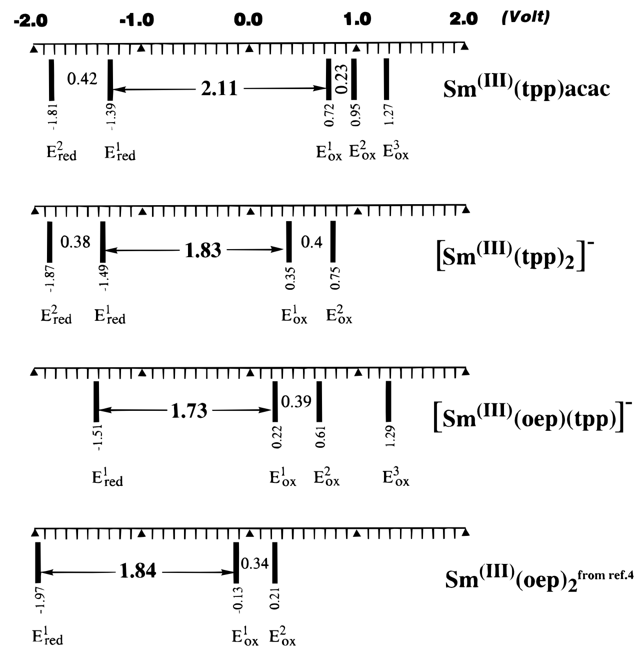

Figure 8. Comparison of electrochemical redox potentials of four samarium(III) complexes.

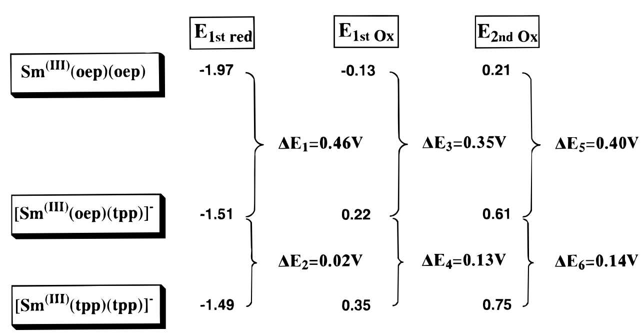

Figure 9. Δ*E* of redox potentials of three samarium complexes.

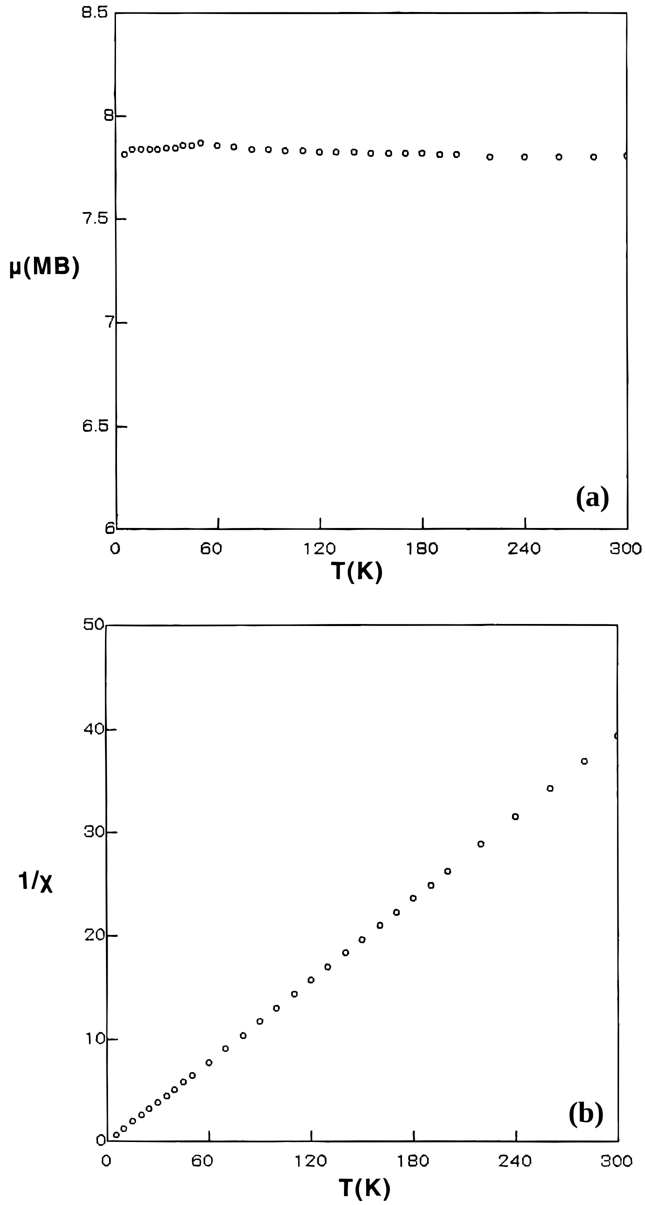

Figure 10. Temperature dependence of magnetic susceptibility of Gd^{III}H(oep)(tpp) complex: (a) μ(MB) versus T(K)n and (b) $1/\chi$ versus T(K).

Table 12. Magnetic Measurement Data for Heteroleptic [Ln^{III}H(oep)(tpp)] (Where Ln = Nd, ..., Tm, except Pm, Yb)

[Ln^{III}(oep)(tpp)]$^-$	μ(300 K) (BM)	μ(5 K) (BM)	μ_{eff} (theor. value)
Nd	3.82	2.90	3.68
Sm	1.62	0.80	1.65
Eu	3.30	0.70	3.40
Gd	7.84	7.80	7.94
Tb	9.86	9.16	9.70
Dy	10.35	9.20	10.60
Ho	10.01	8.82	10.60
Er	9.22	7.80	9.60
Tm	7.40	6.48	7.60

The unique referred similar complex is the [Lu^{III}H(Pc)$_2$], for which the X-ray structure is reported.[50] However, the comparison is not addequate as in this case the proton is completely delocalized over both phthalocyanine rings.

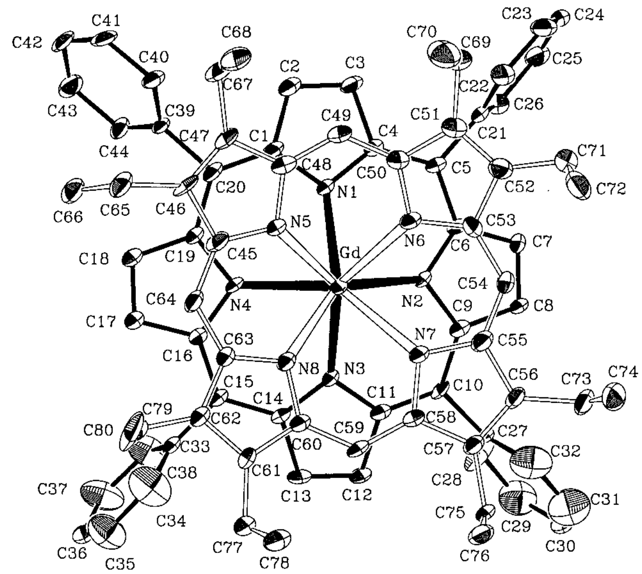

Figure 11. ORTEP diagram of Gd^{III}H(oep)(tpp) at room temperature.

In an attempt to find the position of the hydrogen atom in the difference Fourier map, we collected data at 21 K (see Supporting Information). Unfortunately, we still could not locate it. The mean bond length of Gd−N(tpp) is 2.516 Å and that for Gd−N(oep) is 2.548 Å. The δ_{CN} values at 21 K are 0.245 Å for the tpp and 0.292 Å for the oep. Thus the two macrocycles are now separated by a distance of 3.454 Å, almost 0.05 Å smaller than that found at 298 K. The values for ω_{CN} are 10.93° (tpp) and 13.40° (oep). On the basis of the crystallographic study, we can offer three arguments for the location of the hydrogen atom on the oep ligand. First, the larger doming of the oep ligand at both RT and LT. Second, the mean distance Gd−N(oep) is larger than the mean Gd−N(tpp) distance and there is one Gd−N(oep) distance which is distinctly longer than the other three (Table 2), indicating that the hydrogen is primarly located on the particular nitrogen atom. Third, while on the average the Gd−N distances are shorter at LT, the Gd−N distance to the particular nitrogen on which the hydrogen is primarily localized becomes longer at LT, which is in agreement with the expectation that the hydrogen is more localized at LT than at RT.

Certainly, the above-mentioned arguments could not strongly support by themselves the existence of the H$^+$ on the oep ring. However, these undoubtedly interesting crystallographic data point in the same direction concerning the ring where the H$^+$ in question is favorably sited, as is shown by the total experimental data obtained through the electrochemical and spectroscopical studies reported here and in earlier work.[32] Moreover, the fact that the quantitative results obtained in *solution* through ^{1}H-NMR studies in the diamagnetic member of the Ln homo- and heteroleptic complexes and the data acquired in *solid state* by X-ray crystallography both indicates the oep ring as the favorable H$^+$ site and therefore allow the assignment of H$^+$ to a pyrrole nitrogen of oep macrocycle.

Conclusions

From this study we reach the following conclusions.

(i) The proposed synthetic route and the ensuing purification give rise to neutral double-deckers complexes. Their non-radical character was corroborated by the optical properties as no NIR band and no EPR signal (for free radical) were detected.

(ii) Abstraction of the proton in basic media from the molecule yields deprotonated, non-radical complexes which, also, do not exhibit a NIR absorption band and are EPR silent.

(50) Moussavi, M.; De Cian, A.; Fischer, J.; Weiss, R. *J. Am. Chem. Soc.* **1988**, *27*, 1287−1291.
(51) For coordination number eight (8): Shannon, R. D.; Prewitt, C. T. *Acta Crystallogr., Sect. B: Struct. Crystallogr. Cryst. Chem.*

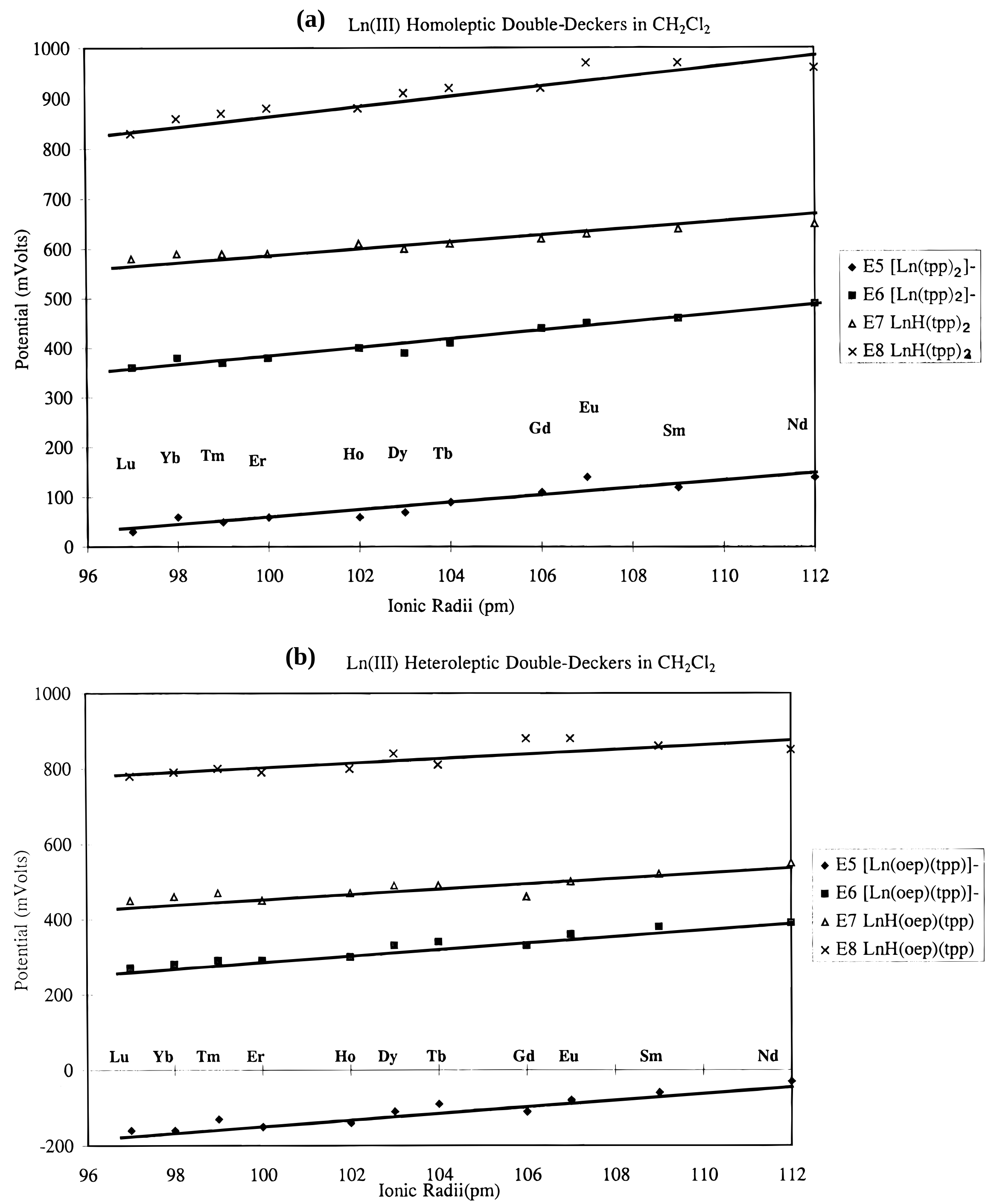

Figure 12. E_5, E_6, E_7, and E_8 electrochemical potentials versus ionic radii for (a) homo- and (b) heteroleptic double-deckers in CH_2Cl_2.

(iii) The strong $\pi-\pi$ interactions between the two macrocycles are essentially confirmed by the UV−visible data in different solvents and by comparison with similar reported data.

(iv) Magnetic succeptibility measurements confirm the oxidation state III for all the heteroleptic derivatives. ESR data show delocalization of the electron spin density from the lanthanide ions to the porphyrin ring, with the exception of Gd(III) and Eu(III) derivatives.

(v) Electrochemical data demonstrate that the electron transfer processes involve molecular orbitals mainly of tpp character. So, tpp which acts formally as a dianion contributes considerably more to the HOMO and LUMO orbitals of the heteroleptic double-deckers. This aspect was confirmed by the IR studies of selected oxidized derivatives (homo- and heteroleptics) as well as by their NIR absorption band. Consequently, the electron deficient chromophore (in the oxidized species) is the tpp ring.

(vi) The electrochemical studies revealed that both forms **A** and **B** (for homoleptic and heteroleptic complexes) were oxidized easier as $\pi-\pi$ interactions increased along the series of lathanide complexes. It was found that all Lu(III) complexes, which possess the smallest ionic radius and consequently were expected to exhibit the smaller interporphyrin distance, oxidized easier (either in the protonated or the deprotonated form) in both solvents CH_2Cl_2 and THF (Figure 12a and b).

(vii) The HOMO−LUMO gap for the heteroleptic complexes was always found to be smaller than the gap in the corresponding homoleptic ones (either oep or tpp) and it decreases as the ionic radius of the central ion decreases and the $\pi-\pi$ interactions increase. As illustrated at Figure 8 for the complexes of Sm(III), the HOMO−LUMO gap for both oep and tpp homoleptic complexes is practically the same. The decrease of the HOMO−LUMO gap in the case of the corresponding heteroleptic Sm(III) complexes manifested mainly by the easier oxidation of the complex. A detailed analysis of all the obtained electrochemical data in THF (where it is possible to measure the HOMO−LUMO gap as electroreduction is observable) clearly indicates that along the Ln series between the electrochemical processes which affect the HOMO−LUMO energy difference, first electrooxidation and first electroreduction, the former exhibits a difference between the hetero- and tpp homoleptic complexes which varies (oxidized easier) from 0.13 (for Sm(III)) up to 0.25 V (forLu(III)), while the latter varies (reduced harder) only from 0.02 (for Sm(III)) to 0.13 V (for Lu(III)). This is the case between the heteroleptic complexes and the oep homoleptic analogous, although the latter are oxidized considerably easier but reduced considerably harder, as well.[4] This results to smaller energy difference between the first electrooxidation and electroreduction processes, hence to a smaller HOMO−LUMO gap.

(viii) The X-ray structure of Gd^{III}(oep)(tpp) in conjunction with reported ^{1}H-NMR data[32] confirm the presence of the proton in the protonated form and that it preferably resides on the more basic oep ring. Consequently, for the heteroleptic ones, the tpp ring could be treated as a dianion and oep as a monoanion.

Acknowledgment. This research was supported by the Greek General Secretariat of Research and Technology through Grant No. 95, No A/A 1946, the Greek General Secretariat of Athletics (OPAP), the Centre National de la Recherche Scientifique and the Paul Sabatier University at Toulouse, France, "Platon" grant for bilateral scientific and technological cooperation (France-Greece) and for G.A.S. the Erasmus Grant ICP-(92/97)-G-2002/13. C.P.R. is grateful to Mrs. A. Athanassiou for financial support. We also thank Dr. Claude Mérriéne from Laboratoire de Chimie Bioorganique et Bioinorganique of Paris XI University for his assistance in recording spectra on the 400 MHz NMR instrument and Prof. C. E. Strouse, UCLA, for the low-temperature X-ray data collection.

Supporting Information Available: For Gd^{III}H(oep)(tpp) at 298 and 21 K, two X-ray crystallographic files, in CIF format, are available. For Gd^{III}H(oep)(tpp) at 298 K: Table S1, summary of crystal, intensity collection and refinement data; Table S2, positional and equivalent thermal parameters of all non-H atoms; Table S3, anisotropic thermal parameters of all non-H atoms; Table S4, bond distances and angles. For Gd^{III}H(oep)(tpp) at 21 K: Table S1, summary of crystal, intensity collection and refinement data; Table S2, positional and equivalent thermal parameters of all non-H atoms; Table S3, anisotropic thermal parameters of all non-H atoms; Table S4, bond distances and angles. Figure S1: EPR spectra of Eu^{III}H(oep)(tpp) complex at room temperature. Figure S2: EPR spectra of (a) $Gd^{III}(oep)_2$, (b) $Gd^{III}H(tpp)_2$, (c) Gd^{III}H(oep)(tpp), and (d) Gd^{III}(tpp)acac complexes. Figure S3: ^{1}H-NMR data for $Lu^{III}H(tpp)_2$ (a) and Lu^{III}H(oep)(tpp) (b) in CH_2Cl_2 and and Lu^{III}H(oep)(tpp) in DMF-d_7. This material is available free of charge via the Internet at http://pubs.acs.org.

IC970879S